CHAPTER 3

Indium Antimonide (InSb): Synthesis, Characterization, and Photocatalytic Activity

InSb has the highest electron mobility and the narrowest direct band gap of all the III-V semiconductors (78000 $cm^2 \cdot V^{-1} \cdot s^{-1}$ and 0.17 eV, respectively).[1] It is attractive for numerous advanced applications such as infrared optoelectronics,[2] photovoltaics,[3] spintronics,[4] and topological quantum computing.[5] Along with the huge exciton Bohr radius of ~60 nm,[6] InSb with the form of NCs is absolutely a fascinating material.

Despite its excellent performance, only a few reports about InSb preparation techniques are available due to its covalent characteristic and air/moisture sensitive nature of precursors. The traditional synthetic routes used in most InSb NCs researches require extreme air-free environments, expensive/hazardous precursors, and high operating temperature, which restrict the advancement of intensive studying on this material. Hence, In order to profit from the advantageous properties of InSb, it is crucial importance to develop the synthetic route of this semiconductor in the simple way.

Here, this chapter reports a new facile route to prepare InSb NCs in an air and at ambient pressure, namely Microwave-assisted Phase Transfer Co-Reduction (MW-PTCR), which reduces many complications implicit to specific equipments and air-free procedures. Spherical cubic zinc blende InSb NCs with an average size of 5 nm were synthesized and spontaneously separated through a rapid microwave-assisted one-pot reaction. The photocatalytic activity of obtained product was investigated by the decolorization of methyl orange dye under NIR, visible light, and UV. The first part of this chapter shows the experiment details on synthesis of InSb NCs, characterization, and photocatalysis method. The latter part of this chapter provides the results and discussions.

3.1 Experiment Methods

Chemicals: Indium chloride ($InCl_3$, 99.9%, Sigma-Alrich), Antimony chloride ($SbCl_3$, 99.9%, Sigma-Alrich), Sodium borohydride ($NaBH_4$, 98%, Alfar Aesar), Ethylene glycol (EG, 99.5%, RCI Labscan), Oleylamine (OAm, 70%, Sigma-Alrich) Bromobenzene (PhBr, Ajax Finechem), Toluene (AR grade, Fisher scitific), and all other common reagent-grade chemicals were obtained from RCI Labscan and Qrec. All chemicals were used as received without further purification.

Equipments: 200 mL Modified flat-flange-end glass vessel (4 cm inner diameter, 18 cm height), Roof-perforated household microwave oven (8 cm hole diameter, Electrolux EMM2009W), and other common laboratory equipment and glassware.

Synthesis of InSb NCs: 50 mL of a 0.04 M EG solution of mixed $InCl_3$ (0.456 g, 2 mmol) and $SbCl_3$ (0.469 g, 2 mmol) was poured into a flat-flange-end 200 mL glass vessel. The solution was heated to 160 °C for 30 minutes to dry and to ensure the complete dissolution of the solids. The solution contained in the glass vessel then was properly placed in a perforated top casing of domestic microwave and the solution was heated cyclically (6 s on and 24 s off) at an operating power of 90 W for 5 minutes (10 cycles). A fine suspension of 1.6 g of $NaBH_4$ (0.04 mol) containing 5 mL of EG, 5 mL of OAm and 30 mL of bromobenzene was added dropwise to the microwave-activated solution inside the microwave chamber. It is noteworthy that the appropriate amount of OAm relative to $NaBH_4$ can benefit the basicity that prevent the oxidation of $NaBH_4$ before reacting with the target ions.[7] During the reaction, the temperature was measured by an infrared detector reading at the surface temperature of Pyrex glass vessels and was found to fluctuate approximately 161 – 168 °C in the upper EG layer and approximately 110 – 115 °C in the lower bromobenzene layer. After the last drop, the microwave was carried out for further 5 minutes to maintain the reaction. The final mixture was left to cool to room temperature under air. Brownish-black colloids were completely transferred to a nonpolar bromobenzene phase within 30 minutes of their visual appearance.

The conventional heating was carried out with the same condition as MW-synthesis. The hot plate and oil bath was applied instead of MW oven.

Post Synthesis Processing: The precipitate is collected by centrifugation and decantation. To further remove impurities, the resulting black paste is resuspended and sonicated in 5mL of toluene and 5mL of dichloromethane is added to precipitate the particles again. The product was then rinsed with warm ethanol to remove NaCl salt and other impurities. After a purification step, the sample was usually suspended in toluene for storage and further characterization. This brownish-black suspension can be redispersed in several nonpolar solvents and greases for many different applications and also be able to deposit easily on several substrates. In case of oleylamine removal, the dispersion was sonicated by vigorous bath sonication for 10 minutes and then centrifuged with acetonitrile.

Characterization: The size, morphology, and microstructure of the nanoparticles were determined by a transmission electron microscope (TEM) (JEM-2010, JEOL, Japan) and by a field emission scanning electron microscope (FE-SEM) (JSM-6335F, JEOL, Japan). Before TEM analysis, the stock dispersion were sonicate for 15 min prior to being dropped onto a TEM copper grid. The elemental analysis was done using energy dispersive spectroscopy (EDS) analysis integrated with a SEM. Phase structures of the material were determined using an X-ray diffractometer (XRD) (MiniFlex 600, Rigaku Denki, Japan) at Cu Kα radiation (λ=1.5406 Å) with a scan step of 0.05° in 2θ and a scan speed of 10°/min. The average diameters were randomly sampling more than 100 particles from SEM and TEM images. Optical absorbance at IR region was recorded using fourier transform infrared spectroscopy (FT-IR) (TENSOR-27, Bruker, Germany) with a resolution of 2 cm^{-1} and scan range of 500 - 4000 cm^{-1}. The sample was prepared by dropping the dispersion of product and toluene on the KBr glass substrate. The band gap was estimated from the absorption peak and the absorption edge was estimated from linear plotting of the following equation: [8,9]

$$(\alpha h\nu)^n = k(h\nu - E_g)$$

Where α is the absorbance, h is Planck's constant, ν is the frequency, n is equal to 2 since InSb is a direct band gap semiconductor, and k is a constant.

Photocatalytical Degradation of MO

The photocatalytic activities of obtained nanoparticles were observed by the degradation of methyl orange (MO) solution under the irradiation of Ninfrared, visible light and UV-light. 20 mg of photocatalyst was suspended in a 100 mL aqueous solution of MO (2 mM). The suspension was kept in the dark for 24 h before irradiation for establishing adsorption–desorption equilibrium. Afterward, the mixture was irradiated with 6 pieces of 5W LEDs light source, which provide the light of wavelength 365-370 nm, 400-800 nm, and 850 nm for the experiment of UV, visible, and NIR, respectively. The lamps were positioned to surround the reaction flask from two sides and top. The control sample was wrapped to protect the light and then carried out in the IR chamber to manipulate the similar environment. All photocatalytic experiments were performed at ambient temperature without bubbling, and the reactor was cooled by fan and water line during the experiment in order to eliminate any heating effects. A 3 mL of working solutions were sampled at given time intervals. The degraded solutions were analyzed using UV–Vis spectrophotometer (Lambda 25, Perkin Elmer, USA), and the absorption peak at 461 nm was monitored. The decolorization percentage of MO was calculated by the following equation:

$$\eta = \frac{C_0 - C}{C_0} = \frac{A_0 - A}{A_0} \times 100\%$$

Where η is the decolorization percentage, C_0 is the initial concentration, C is the concentration at any time, A_0 and A are the initial and instantaneous absorbency of MO solution at 461 nm, respectively.

Photocatalytic Inactivation of Bacteria

Colony-Forming Capability Test: This suspension test measures the bactericidal effect of the material and makes it possible to determine the photocatalytic effect for the reduction in the bacterial colonies. Gram-negative *Escherichia coli* (*E. coli*) and gram-positive *Staphylococcus aureus* (*S. aureus*) were chosen to conduct a pure culture study in suspension. The sample suspension consisted of proper concentration of bacteria and 20 mg of photocatalyst was exposed to light from 6 pieces of 5W LEDs; visible region (400-800 nm) and NIR (850 nm) for Vis and NIR experiment section, respectively.

After 1 h of irradiation, the suspensions were diluted from 10 to 10^5 fold of concentration, each of which was incubated on agar plate for 24 h before counting the colonies. The experiment was divided into two groups, *E. coli* and *S. aureus*. Each group contained 4 samples; kept in the dark, exposed with visible light, exposed with NIR, and control. The control sample for these tests contained no catalyst.

Agar Diffusion Method: Agar plates were prepared using nutrient agar plate mixed and the 20 mg powder samples of InSb@OAm. The agar was autoclaved at 120 °C prior to testing. After autoclaving the agar was heated to 100 °C and the photocatalyst was added to the molten agar. Each of the agar plates were inoculated with 50 µL *E. coli* and 50 µL of *S. aureus* suspension. Each plate was prepared in duplicate with one sample irradiated with the same NIR reactor described above and one sample kept in the dark. After irradiating the samples for 1 h, both sets of plates were incubated at room temperature for 24 h to allow any growth of the bacteria to take place.

3.2 Results and Discussions

MW-PTCR Route for InSb NCs

Figure 1 shows the TEM images for as-prepared product after purification and after isolation from support matrix. The presence of InSb nanoparticles supported on the OAm network (InSb@OAm) in Figure 3.1a indicates that The InSb NCs was originally obtained in organic-coated form. The passivation process of NCs by OAm was occurred during the reaction. After isolation, it can be seen clearly that the prepared InSb NCs are nearly monodispersed with a spherical uniform size of 5 nm (Figure 3.1b). This result is benefited from the passivation process, which the crystal growth and Ostwald ripening process were prevented from the freshly prepared NCs. Crystal structure of individual InSb NC was further examined by high resolution TEM (HRTEM) and the result was shown in Figure 3.1c. The interplanar distance between the adjacent lattice fringes was observed as a value of 3.76 Å, which is corresponding to the oriented (111) plane of the cubic zinc blende InSb.

The crystal structure of obtained product was further characterized by powder XRD. Figure 2 depicts the diffraction patterns of as-prepared sample (a) and the purified sample (b). The characteristic Bragg peaks of obtained NCs were interfered by the reflection of organic layer and results in noisy pattern. However, all diffraction peaks of purified sample were fully matched with the characteristic diffraction pattern of bulk zinc blende InSb (Black vertical line, JCPDS No. 6-208, a = 6.4782 Å), in which no impurities such as In, Sb or oxide phases can be detected. A blue shift of the diffraction pattern was observed, which indicates that the particle size are smaller than its Bohr radius and result in slightly increased cell parameters and d-spacing.[10] The Removal of impurities was confirmed by the disappearance of a peak at $2\theta = 32.8°$, which is consistent with characteristic peak of metallic In. The crystallite sizes of ~5 nm and spherical morphology of purified In@OAm sample were confirmed by SEM image that shown in Figure 3.3. The surface appearance shows clearly the cross-connection of outer organic layer and small salient feature of InSb NCs. The corresponding EDS analysis also verified the nearly 1:1 InSb composition.

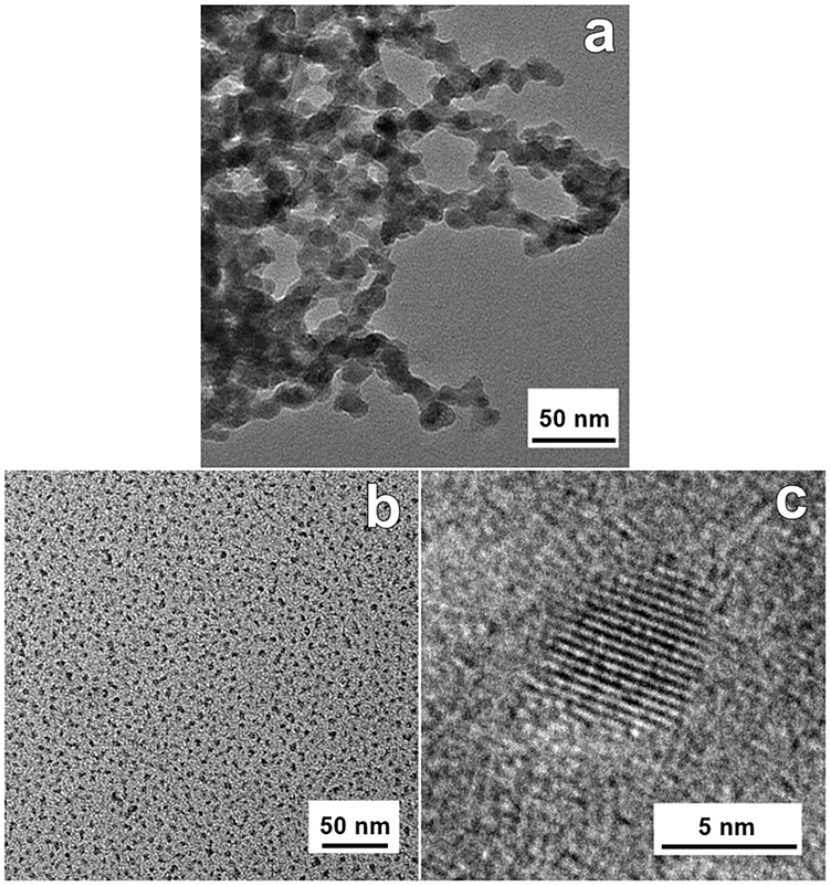

Figure 3.1 The TEM images of as-prepared InSb NCs (a), isolated InSb NCs (b), and HRTEM image of individual InSb crystal (c).

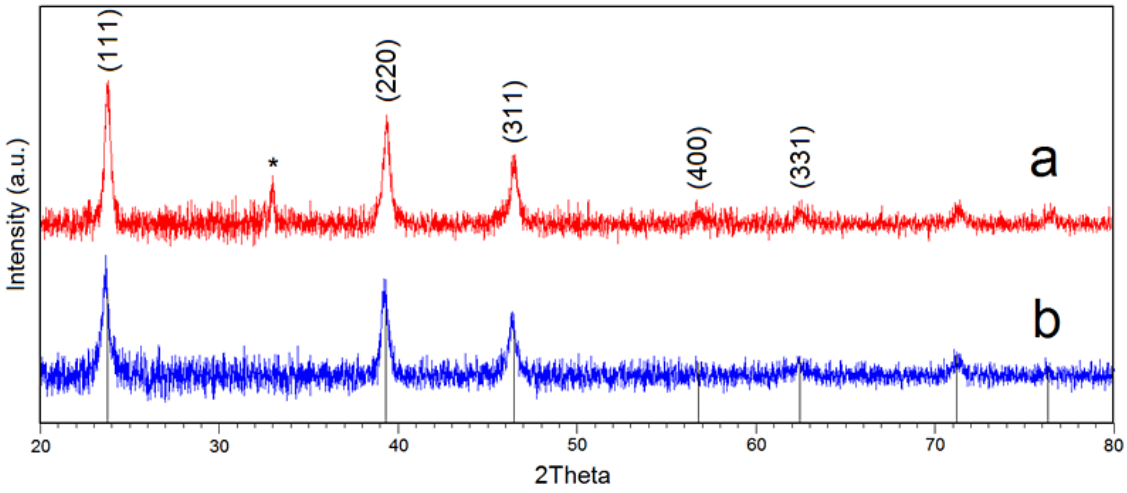

Figure 3.2 X-ray diffraction patterns of the as-prepared product before (a) and after (b) purification. Asterisk marked is referred to the metallic indium.

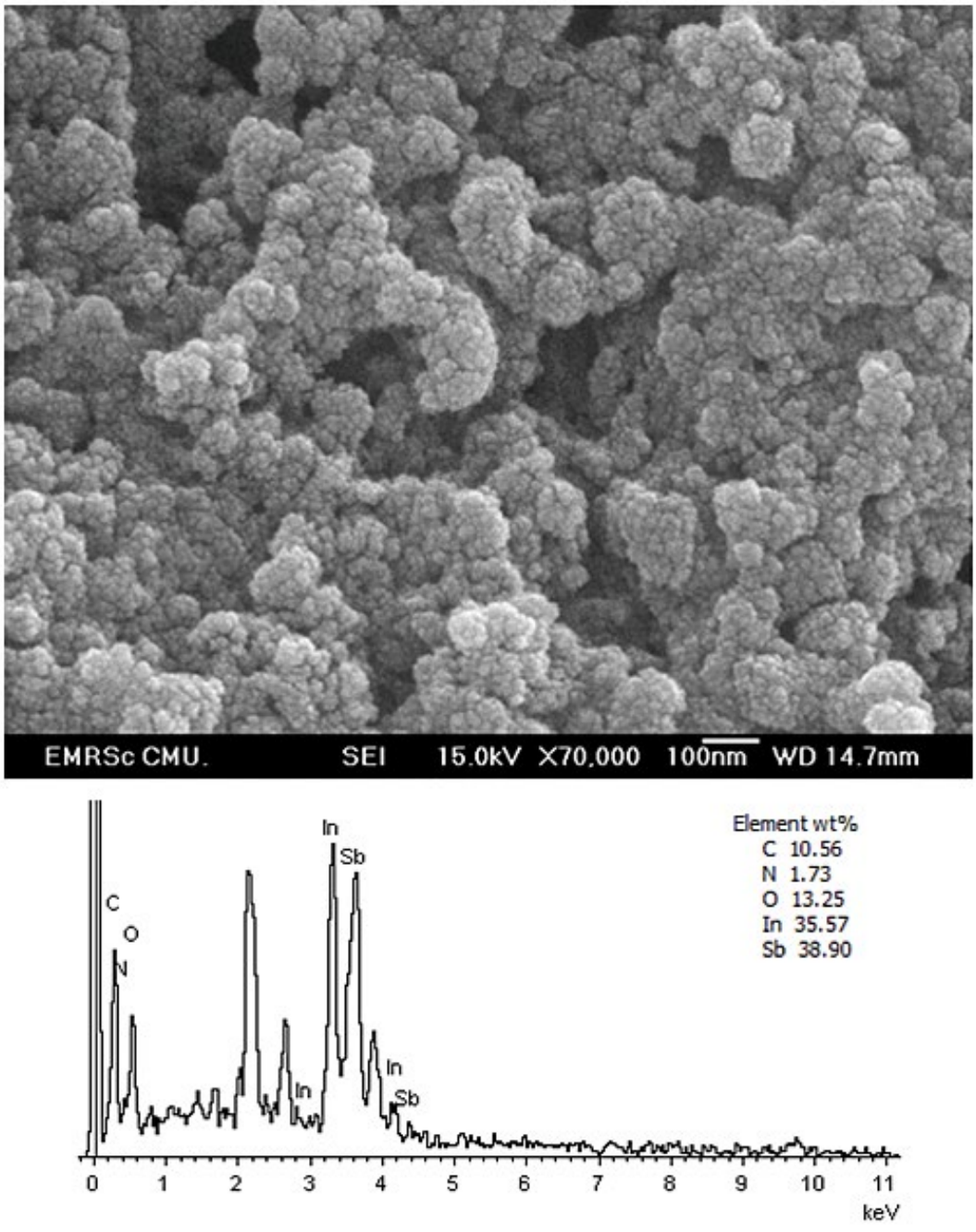

Figure 3.3 The SEM image of InSb@OAm and correspondence EDS spectrum. Oxygen content is corresponding to residue EG and partial oxide species at the surface.

All the above results led us to believe that the InSb NCs were successfully synthesized and were obtained firstly in organic-capped form with slightly metallic In impurity. Pure phase InSb NCs could be achieved by post synthesis treatment as described in experiment section.

In our method, the reaction mechanism is proposed to occur via three steps. First, the constituent ions in the starting solution were uniformly activated upon exposure to the MW radiation. Active indium ions were closely arranged with antimony ions because of their similar ionic radii and ionicity. Thus, when the reducing agent was introduced, the InSb NCs had burst conveniently from the co-reduction of both arranged indium and antimony ions. Second, the surface binding of OAm to the NCs was subsequently formed to reduce the surface energy of the NCs. This process not only stabilizes the freshly prepared NCs, but also prevents both aggregation and oxidation phenomenon. Finally, the phase transfer process was driven efficiently by the MW radiation generating a large temperature gradient between the strongly MW-absorbing medium (EG) and the nearly MW transparent solvent (bromobenzene). Individual organic-capped NCs rapidly migrated to nonpolar phase and also avoided the growth environment. In fact, by using an appropriately dense non-aqueous phase liquid (DNAPL) such as bromobenzene, the autogenous NC transfer was also gravitationally controlled to the denser nonpolar phase. Thus, the freshly synthesized InSb NCs had moved away from the risky reoxidation environment and migrated downward with nearly the same growth histories.

To investigate the system behavior, chemical parameters including precursor ratio, reducing ratio, and OAm volume were varied to compare with the main condition described above. The varied condition and the results were summarized briefly in Table 3.1.

Table 3.1 Summary of results and conditions used in MW-PTCR method for InSb NCs

Sb/In ratio†	$NaBH_4$/In ratio†	OAm volume [mL]	Product(s)	Average size of InSb (nm)
0.75	20	5	InSb + In	11
1.25	20	5	InSb	6
1	10	5	InSb	12
1	30	5	InSb	4
1	20	2.5	InSb	14
1	20	10	InSb	5

†Standard amount of Indium precursor is 2 mmol.

By maintain the staring solution at 50 mL, the reducing of starting Sb^{3+} concentration results in the increasing of metallic In phase. The reason is the excess indium ions can be reduced to form metallic phase and then it was precipitated together with InSb inside the organic shell. On the other hand, the excess Sb^{3+} did not result in the opposite way because freshly reduced metalloid Sb^0 cannot participate with the OAm network Sb^0 and tends to redissolve into the solution.[11] This behavior is confirmed by the forming of opaque white precipitate of antimony oxide species on EG layer when the EG solution was left in air atmosphere for more than 2 h.

The reducing agent concentration affects directly to the final InSb particle size. This influence is entirely understandable because the nucleation rate is depended on the amount of reducing agent in the system. When the lesser concentration is introduced, it means the lesser nucleation rate. Hence, with the steady growth rate, the larger particle will be obtained. However, increasing the $NaBH_4$/In ratio more than 20 did not produce the significant difference in size.

The particle size is also affected by the amount of stabilizing agent (OAm). It can be seen clearly that when the OAm volume was reduced by 2, the average crystallite size was dramatically increased to 14 nm. The key explanation is the overall passivation rate by OAm was dropped when the lower OAm concentration was applied. The slower passivation rate leads the more growth time of crystal seed and then result in larger particle achieved.[12] However, applying higher amount of stabilizer more than 5 mL did not lead us to achieve smaller particles. It is probably because the maximum rate was reached already at the condition using 5 mL OAm. In contrast, too much OAm caused the bulky and viscous paste that brought more complicated purification step.

Along with the MW-assisted synthesis, the similar procedure was carried out with conventional heating to investigate the efficiency of each method. Figure 3.4 shows the TEM image of InSb product obtained from convention heating experiment. It can be seen clearly that the obtained product was contained with spherical polydisperse particles by a size range of 20 – 80 nm. The small particle was still caged inside the organic matrix, but the larger particle was bound at the surface of polymer. This vision indicates evidently the unequal growth histories of particles. The assumption is that, at the prior state, the all small crystals might be stabilized by the OAm matrix, but the

growth process and Ostwald ripening was not separated due to the temperature difference between the reaction layer (EG) and resting layer (Bromobenzene) is negligible. Thus, some seed crystals became larger and left the stabilization layer to further growth. At last, the polydisperse nanoparticles were obtained.

All the above facts can be realized that the novel MW-PTCR method can be used efficiently to produce the InSb NCs

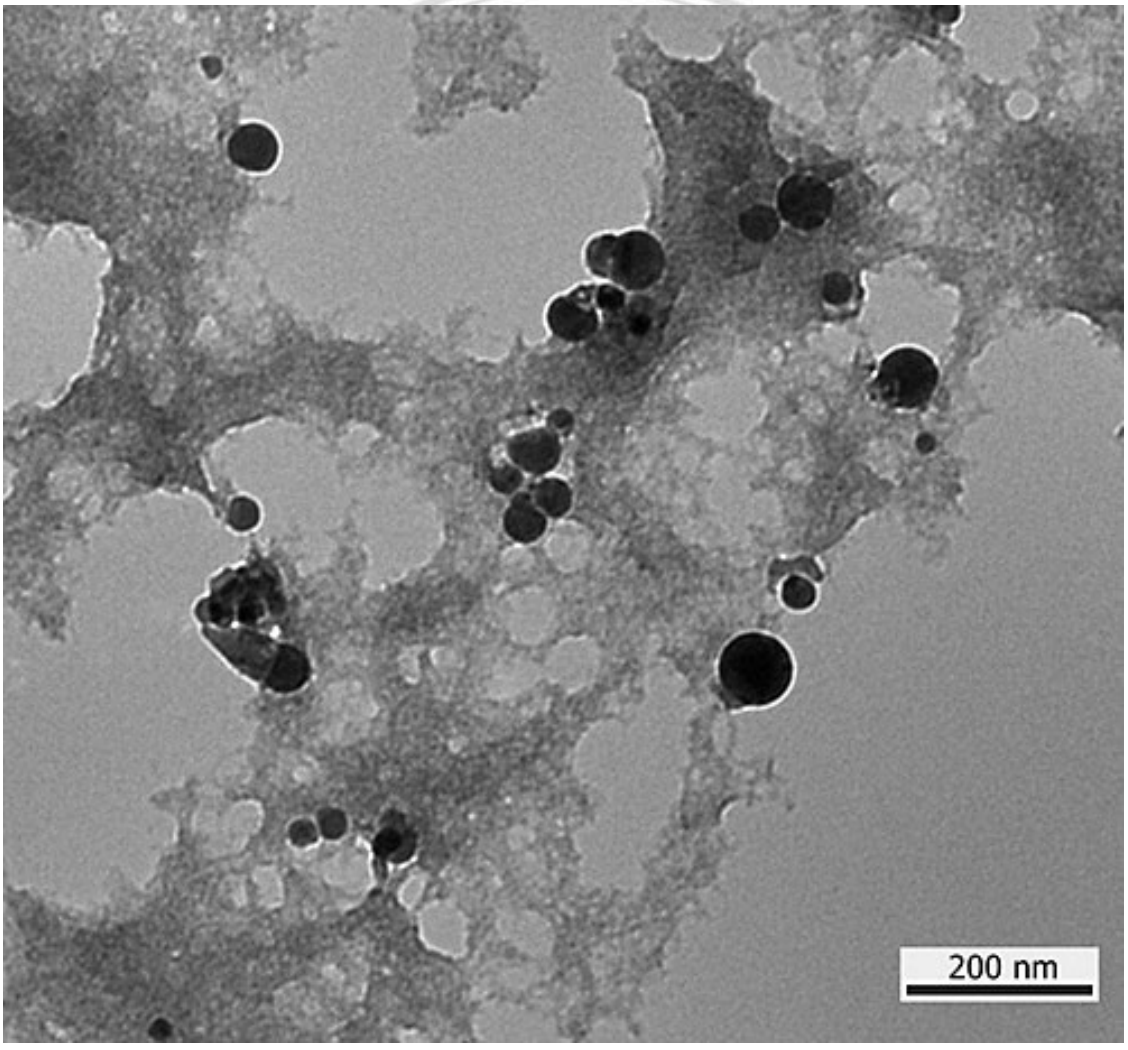

Figure 3.4 TEM image of InSb obtained from conventional heating

Optical Property and Photocatalytic Activity

For a narrow band gap semiconductor, the infrared absorption edge is relevant to the energy band of semiconductor catalyst. The FT-IR spectrum was performed to investigate the band gap (E_g) of obtained products in the wavelength in which the energy band gap is located. The Fig 3.5 shows the infrared absorbance spectrums of InSb@OAm (a), isolated InSb NCs (b), and referenced toluene (c). A prominent absorbance curve near 2.94 μm, which corresponds to the energy of 0.422 eV, can be seen in both InSb@OAm and isolated InSb sample. This value is much larger than that 0.17 eV of the bulk InSb due to the blue shift effect that normally founded on tiny particles. However, another sharp peak around 6.10 μm, which corresponds to the energy of 0.203 eV, was also appeared in embed sample. This band is much closer to that bulk's value. Since this adsorption peak is observable in only capped sample, it might be the adsorption of the larger particles caged inside the oleylamine matrix or the interference adsorption from organic domain.

It is known that the optical band gap for direct interband transitions and the absorption coefficient (α) near the absorption edge has a relationship that complied with the equation described above. The optical band gap for the absorption edge can be obtained by extrapolating the linear portion of the plot $(\alpha h\nu)^2$ vs $h\nu$ to $\alpha = 0$.[13] The relationship between $(\alpha h\nu)^2$ and $h\nu$ was plotted in the Figure 3.6. Unfortunately, there is no significant difference between the plotted spectrum of (a) and (b). The absorption edges derived from the linear fit is estimated as 0.20 eV, which is mismatched to that major absorbance peak of both sample. However, it is consistent to the value obtained from minor absorbance peak of embed sample, which is seems to be lesser affected by quantum behavior. From this result, the 'actual' band gap of synthesized NCs is still unclear due to the behavior of some phenomenon when the particular particle's size is smaller than that Bohr's radius such as quantum confinement and Burstein-Moss shift. The initial band gap of obtained products are pointed out around 0.20 – 0.45 eV, while the further analysis is still underway.

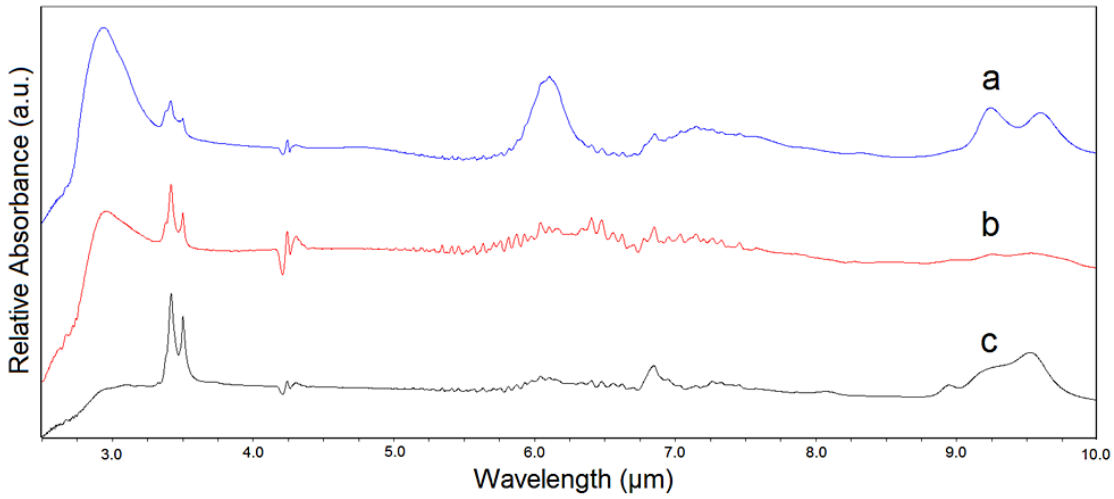

Figure 3.5 FTIR spectrums of (a) InSb@OAm, (b) isolated InSb, and (c) reference toluene.

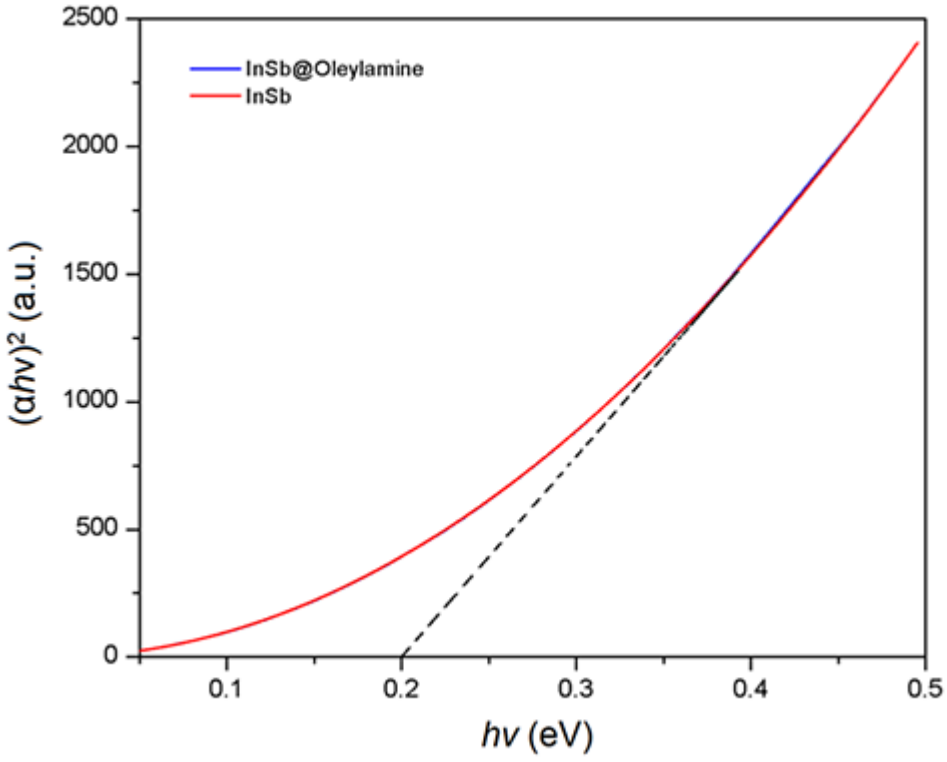

Figure 3.6 $(\alpha h\nu)^2$ vs $h\nu$ plot for InSb@OAm and isolated InSb NCs. The linear fitted appear in dashed line

Figure 4 shows the decolorization rate of control and exposed samples. It can be seen clearly that the degradation of MO was increased significantly by the increase of irradiation time of all lighting source. Over 50% of MO degradation can be observed within 15 minutes of exposure for NIR and at 30 minutes for both UV and visible light. After 1 h of irradiation, the decolorization percentage of MO solution reached 97.6%, 85.7%, and 83.6% by using NIR, UV light, and visible light, respectively. Although about 16.2% of non-photoinduced degradation was observed in control sample, the exposed sample shows more than 65% higher than the adsorption in dark. This result suggests that the MO solutions could be photocatalytically decolorized over synthesized catalyst. Not only the NIR can be utilized, but UV and visible light also can be employed with this catalyst. This performance promoted our material to be a part of novel solar energy utilization. However, to clarify further nature of a catalyst, elaborative studying in additional details is needed.

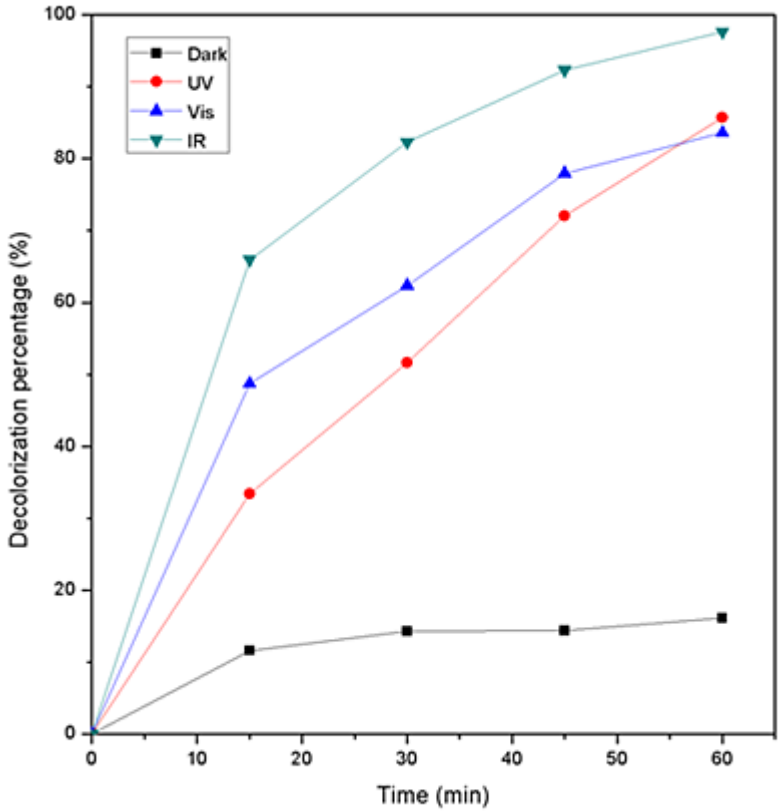

Figure 3.7 The decolorization rates of MO over InSb@OAm with different light source.

Table 3.2 Concentrations of the *E. coli* and *S. aureus* suspension test for the reference and test samples of InSb@OAm.

Samples		10 – fold serial dilutions					Total bacteria (CFU/mL)
		10^{-1}	10^{-2}	10^{-3}	10^{-4}	10^{-5}	
E. coli	Control	>600 colony			121	10	1.2×10^{6}
	InSb dark	14	0	0	0	0	1.4×10^{2}
	InSb. vis	22	0	0	0	0	2.2×10^{2}
	InSb. IR	7	1	0	0	0	7.0×10^{1}
S. aureus	Control	>600 colony			92	4	9.2×10^{5}
	InSb dark	15	4	0	0	0	1.5×10^{2}
	InSb. vis	4	2	0	0	0	4.0×10^{1}
	InSb. IR	4	0	0	0	0	4.0×10^{1}

The bactericidal ability of InSb@OAm was observed in colony-forming test. Table 3.2 shows the colony forming units (CFU) per mL of culture solutions. Approximately one million CFU can be seen clearly in both control samples, whereas the less than three hundred CFU can be observed in all InSb@OAm-contained samples. The inhibition of bacterial growth was occurred even the light is not activated (see 'InSb dark' section). This result suggests that the both gram-negative and gram-positive bacteria might be poisoned by InSb@OAm and result in the low CFU value. Thus, it seems difficult to separate precisely between the effect of toxicity and photocatalytic inactivation from the result of *E. coli* section. However, the results from gram-positive *S. aureus* imply the significant difference between the irradiated and non-irradiated sample. The cooperation results with NIR and visible light exhibit the lower CFU than the kept-in-dark sample. This evidence indicates that the photocatalytic effect was occurred over the InSb@OAm photocatalyst.

The further investigation was conducted with agar diffusion method. Figure 3.8 shows the photographs of disk diffusion results after 24 h of incubation. The left half of the photograph fragments is the non-irradiated samples and the right half is the NIR-irradiated sample, where the top half section represents the *E. coli* samples and the bottom half displays the *S. aureus* samples. The zone of inhibition on the *E. coli* disks was observed even the light was screened. This result agrees well with the previous

experiment on colony-forming test that the growth of gram-negative *E. coli* was inhibited by InSb@OAm itself, and the experiment on this bacterium cannot describes exactly the photocatalytic activity of our material. With the same way, the significant result was found on the gram-positive *S. aureus* sample. The NIR-irradiated sample presents the clearer inhibition zone than the dark-control sample. This result may indicate that the rate of bactericidal process was photocatalytically enhanced by NIR, and InSb@OAm was photocatalytically active under NIR radiation.

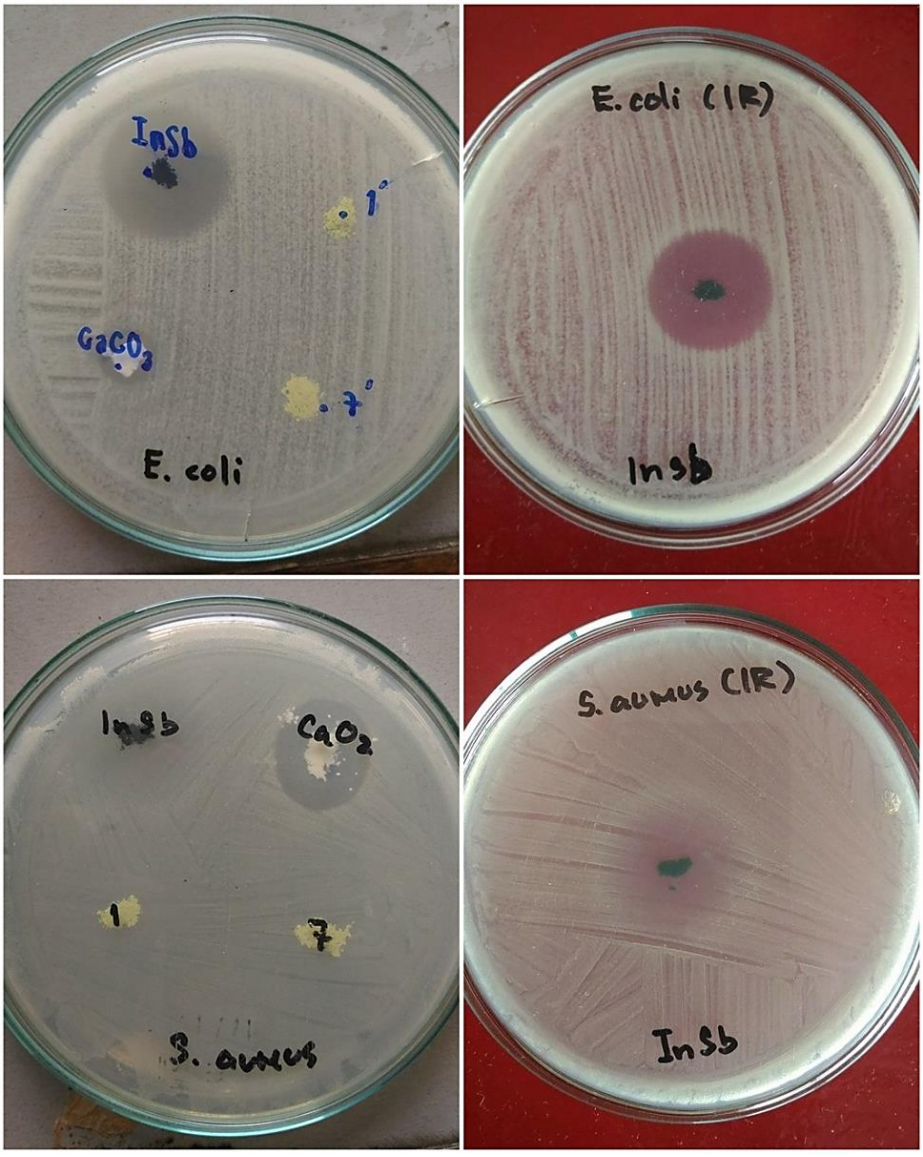

Figure 3.8 Photographs of disk diffusion (zone of inhibition) results before (left side) and after (right side) NIR irradiation. Top section is *E. coli* and bottom section is *S. aureus*.

These preliminary experiments on photocatalytic inactivation of bacteria confirm the photocatalytic activity of InSb@OAm. However, the mechanism of growth inhibition is not only the effect from purely photocatalysis but also the other physical-biological factors of cell and material. Since the InSb@OAm contains the heavy metal indium, the catalyst might be toxic for bacteria. The thinner peptidoglycan layer of gram-negative bacterium might be poisoned easily than that thicker cell wall of gram-positive species and result in unidentified effect of inactivation. The further studies on bactericidal property of this material with the intensive experiment design would be published elsewhere.

3.3 Conclusion

In summary, we report on a novel method called microwave-assisted phase transfer co-reduction (MW-PTCR) for the synthesis of InSb NCs. Spherical ~5 nm InSb NCs were successfully synthesized with the assistance of oleylamine stabilization and an autogenous phase transfer strategy. The synthesized products can be used as an excellent photocatalyst that use the energy from the region of NIR to UV to decompose methyl orange dye and use the NIR and visible light to inhibit the growth of bacteria. This work stands at a previously unexplored intersection of microwave-assisted synthesis, InSb III-V semiconductor materials, and NCs preparation strategy, each of which represents an important current issue in material synthesis. To the best of our knowledge, this simple and scalable synthesis routes approach is the first colloidal method for the preparation of InSb that is performed in air and at ambient pressure. We anticipate that our practical protocols comprise the initial advances in a fertile area of material chemistry.

References

[1] Abautret, J., Perez, J. P., Evirgen, A., Rothman, J., Cordat, A., & Christol, P. (2015). Characterization of midwave infrared InSb avalanche photodiode. *Journal of Applied Physics*, 117(24), 244502.

[2] Hoffmann, M. C., Hebling, J., Hwang, H. Y., Yeh, K. L., & Nelson, K. A. (2009). Impact ionization in InSb probed by terahertz pump—terahertz probe spectroscopy. *Physical Review B*, *79*(16), 161201.

[3] Beek, W. J., Wienk, M. M., & Janssen, R. A. (2006). Hybrid solar cells from regioregular polythiophene and ZnO nanoparticles. *Advanced Functional Materials*, *16*(8), 1112-1116.

[4] Žutić, I., Fabian, J., & Sarma, S. D. (2004). Spintronics: Fundamentals and applications. *Reviews of modern physics*, *76*(2), 323-410.

[5] Nayak, C., Simon, S. H., Stern, A., Freedman, M., & Sarma, S. D. (2008). Non-Abelian anyons and topological quantum computation. *Reviews of Modern Physics*, *80*(3), 1083-1159.

[6] Yoffe, A. D. (2002). Low-dimensional systems: quantum size effects and electronic properties of semiconductor microcrystallites (zero-dimensional systems) and some quasi-two-dimensional systems. *Advances in Physics*, *51*(2), 799-890.

[7] Liu, B. H., & Li, Z. P. (2009). A review: hydrogen generation from borohydride hydrolysis reaction. *Journal of Power Sources*, *187*(2), 527-534.

[8] Yang, M. H., Yang, M. C., & Sun, I. W. (2003). Electrodeposition of indium antimonide from the water-stable 1-ethyl-3-methylimidazolium chloride/tetrafluoroborate ionic liquid. *Journal of The Electrochemical Society*, *150*(8), C544-C548.

[9] Zhang, X., Hao, Y., Meng, G., & Zhang, L. (2005). Fabrication of highly ordered InSb nanowire arrays by electrodeposition in porous anodic alumina membranes. *Journal of the Electrochemical Society*, *152*(10), C664-C668.

[10] Biefeld, R. M. (2002). The metal-organic chemical vapor deposition and properties of III–V antimony-based semiconductor materials. *Materials Science and Engineering: R: Reports*, *36*(4), 105-142.

[11] Johnson, C. A., Moench, H., Wersin, P., Kugler, P., & Wenger, C. (2005). Solubility of antimony and other elements in samples taken from shooting ranges. *Journal of Environmental Quality*, *34*(1), 248-254.

[12] Sun, S., & Zeng, H. (2002). Size-controlled synthesis of magnetite nanoparticles. *Journal of the American Chemical Society*, *124*(28), 8204-8205.

[13] Kuriyama, K., Takahashi, Y., & Sunohara, F. (1993). Optical band gap of Zn 3 N 2 films. *Physical Review B*, *48*(4), 2781.